LETTERS

Evidence for a terminal Pt(IV)-oxo complex exhibiting diverse reactivity

Elena Poverenov[1], Irena Efremenko[1], Anatoly I. Frenkel[3], Yehoshoa Ben-David[1], Linda J. W. Shimon[2], Gregory Leitus[2], Leonid Konstantinovski[2], Jan M. L. Martin[1] & David Milstein[1]

Terminal oxo complexes of transition metals have critical roles in various biological and chemical processes[1,2]. For example, the catalytic oxidation of organic molecules[3,4], some oxidative enzymatic transformations[5–7], and the activation of dioxygen on metal surfaces[8] are all thought to involve oxo complexes. Moreover, they are believed to be key intermediates in the photocatalytic oxidation of water to give molecular oxygen, a topic of intensive global research aimed at artificial photosynthesis and water splitting[9–13]. The terminal oxo ligand is a strong π-electron donor, so it readily forms stable complexes with high-valent early transition metals. As the *d* orbitals are filled up with valence electrons, the terminal oxo ligand becomes destabilized[2]. Here we present evidence for a d^n ($n > 5$) terminal oxo complex that is not stabilized by an electron withdrawing ligand framework. This d^6 Pt(IV) complex exhibits reactivity as an inter- and intramolecular oxygen donor and as an electrophile. In addition, it undergoes a water activation process leading to a terminal dihydroxo complex, which may be relevant to the mechanism of catalytic reactions such as water oxidation.

To date, the very few terminal oxo complexes having more than five valence *d* electrons are all stabilized by powerful electron accepting ligands: namely $NaRe^{(I)}(O)(PhCCPh)_2$, in which extensive back bonding to the alkyne ligands was noted[14], and complexes stabilized by the encapsulating, highly effective π-accepting polytungstate ligand, including $Pt^{(IV)}$ (ref. 15), $Pd^{(IV)}$ (ref. 16) and Au (ref. 17). A d^5 Fe(III) oxo complex stabilized by a protective hydrogen bond cavity has been reported[18]. Isolation of a terminal d^6 metal-oxo complex not bearing strong electron withdrawing groups is desirable, as it may provide insight into the reactivity potential of the metal-oxo bond, in addition to information regarding spectroscopic and structural aspects. Particularly desirable are terminal oxo complexes of platinum, as this metal and its compounds are widely used by industry in oxygen-based technologies. Towards this goal, we have used a pincer complex of platinum.

Pincer complexes, involving a meridional, tridentate ligand framework, are of considerable current interest, owing to the structural versatility of such systems, leading to a variety of bond activation and catalytic processes[19]. Reaction of the cationic pincer PCN Pt complex **1a** (PCN = $C_6H_3[CH_2P(t\text{-}Bu)_2](CH_2)_2N(CH_3)_2$; ref. 20) with a freshly prepared acetone solution of dioxirane[21] resulted in immediate formation of a new complex, formulated as the terminal oxo complex **2** (Fig. 1a). The $^{31}P\{^1H\}$ NMR spectrum of **2** shows a singlet at 64.27 p.p.m. with Pt satellites (coupling constant $J_{Pt\text{-}P} = 2{,}686$ Hz) and the $^{195}Pt\{^1H\}$ NMR spectrum exhibits a signal at −645.88 p.p.m. (broad doublet, $J_{P\text{-}Pt} = 2{,}686$ Hz), definitely indicating a Pt(IV) oxidation state (for comparison, the chemical shift of the starting Pt(II) complex **1a** is −4,015 p.p.m.). (Here $\{^1H\}$ indicates proton-decoupled.) In the $^{13}C\{^1H\}$ NMR spectrum, the *ipso* carbon gives rise to a doublet at 147.25 p.p.m. ($J_{P\text{-}C} = 5$ Hz), and in the $^{19}F\{^1H\}$ NMR spectrum, the outer-sphere BF_4 anion gives rise to a singlet at −149.87 p.p.m. The NMR data exclude the possibility of the corresponding (PCN)Pt(OH) complex, which has a completely different NMR pattern[20]. Electrospray mass spectrometry analysis is in line with the structure of **2**, indicating two signals at mass/charge ratios m/z^+ 518.07(M+1) and m/z^- 87.29 (BF_4). The infrared spectrum in acetone solution shows an absorption at 783 cm^{-1}, which is in the range expected for Pt=O vibration (Supplementary Fig. 4)[22].

To exclude a dimeric $[(PCN)Pt(\mu\text{-}O)]_2$ structure, PGSE (pulsed gradient spin echo) NMR studies were performed in acetone-d_6. Diffusion coefficients (*D*) and hydrodynamic radius (*r*) of complex **2** and, for comparison, complex **3** (see below) were determined, giving $D = 1.078 \times 10^{-9}$ m^2 s^{-1}, $r = 6.1$ Å for **2**, and $D = 1.186 \times 10^{-9}$ m^2 s^{-1}, $r = 5.6$ Å for **3**. Both the absolute *D* and *r* values of

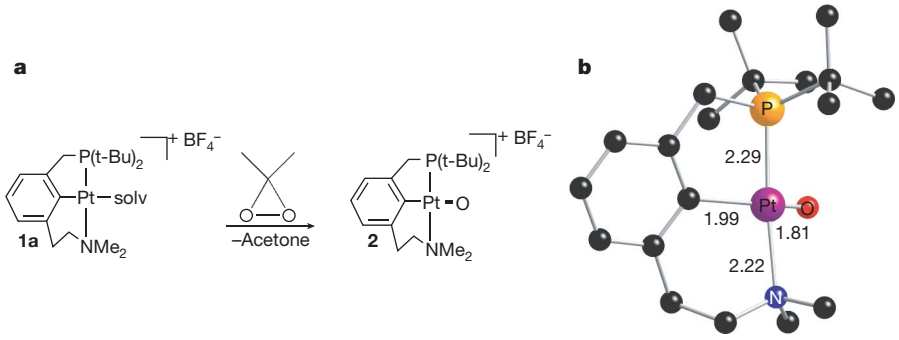

Figure 1 | Preparation and DFT structure of complex 2. a, Preparation of complex **2** by reaction of the Pt(II) complex **1a** with dioxirane. **b**, DFT structure of complex **2** optimized at the PBE0/pc1 level of theory (hydrogen atoms are omitted for clarity).

[1]Department of Organic Chemistry, [2]Unit of Chemical Research Support, The Weizmann Institute of Science, Rehovot 76100, Israel. [3]Department of Physics, Yeshiva University, New York, New York 10016, USA.

complex **2** and their good similarity to that of the unambiguously monomeric **3** clearly indicate the monomeric structure of **2** (ref. 23), as also strongly indicated by density functional theory (DFT) calculations, which show that it is impossible to obtain a Pt(IV) μ-oxo dimer, or a μ-hydroxo-dimer, starting from complex **2** because of severe steric constraints. The radius obtained by rotating the DFT structure of **2** (see below) about its geometric centre is 6.06 Å, in correlation with the experimental hydrodynamic radius. The diverse reactivity of complex **2** is commensurate with its monomeric structure (see later).

DFT studies performed on complex **2** show that the reaction **1a** → **2** is thermodynamically favourable ($\Delta G^0_{298} = -11.1$ kcal mol^{-1} in acetone solution). According to the calculations, the optimized structure of **2** adopts a distorted square planar geometry with the oxygen atom being 35.3° out of the C–Pt–P plane (Fig. 1b). The calculated Pt–O bond length (1.811 Å) is unambiguously shorter than typical Pt(IV)–OH single bonds, which are in the range 1.943–2.079 Å (based on the Cambridge Structural Database), but it is longer than that reported[15] for $K_7Na_2[O{=}Pt(H_2O)(PW_9O_{34})_2]$, 1.720 Å. Analysis of the covalent part of the Pt–O bonding in complex **2** shows that the low stability of electron-rich terminal oxo complexes can be attributed to occupation of strongly antibonding Pt–O π* molecular orbitals. The non-planar geometry of the complex decreases the overlap between metal-ligand orbitals, reducing this unfavourable occupation. The phenyl group serves as an electron donor, and no backdonation to it takes place because of the high energy of the vacant phenyl orbitals (Supplementary Fig. 2 presents a simplified molecular orbital diagram), as supported also by a comparison of natural bond orbital charges in **2** and **1** (Supplementary Fig. 3). According to the DFT calculation, acetone coordination is unfavourable (see Supplementary Information).

The local atomic environment and charge state of Pt in complex **2** were investigated by two methods of X-ray absorption spectroscopy, namely, extended X-ray absorption fine structure (EXAFS) and X-ray absorption near edge structure (XANES).

XANES data (Fig. 2a) of **2** and other compounds used for calibration (complexes **1a** (solv = H_2O), **1c** and **4** (Fig. 3) as well as Pt foil) confirmed the nominal charge states of Pt in all the complexes. The observed differences in the *d*-hole density which is proportional to the absorption peak area are consistent with the difference in the formal valences of Pt in complexes **2** and **4** (4+), **1a** and **1c** (2+) and Pt foil (0).

Analysis of EXAFS data in the four complexes was performed self-consistently by imposing constraints dictated by our X-ray diffraction and DFT analyses: for example, we assumed that the lengths of Pt–P, Pt–N, Pt–C, Pt=O, Pt–OH and Pt–OH_2 bonds are unique and do not significantly depend on a particular complex. By using such a 'fingerprinting' approach, we obtained partial contributions χ_{Pt-OH}, χ_{Pt-OH_2} and $\chi_{Pt=O}$ to EXAFS data of these complexes. These three types of platinum–oxygen bond were found to have very different strengths: Pt=O is the stiffest, Pt–OH_2 the weakest and Pt–OH the intermediate in strength between the two former bonds, as intuitively expected (Fig. 2b). Our results demonstrate that the Pt=O peak maximum is shifted to the left relative to the Pt–OH peak maximum (Fig. 2b, inset) by approximately 0.1 Å, in agreement with our DFT calculations described above, which indicate that the Pt=O in **2** differs from the Pt–OH in complex **4** (see below) by 0.14 Å (at the PBE/sdd level). FEFF6 calculations of the theoretical EXAFS signal for the DFT model of complex **2** are in qualitative agreement with the DFT calculations.

Complex **2**, which has no significant electron accepting framework that can stabilize the terminal oxo ligand, exhibits diverse reactivity (Fig. 3). Initially, we explored its oxygen transfer reactivity. Reaction of **2** with PPh_3 at room temperature resulted in quantitative formation of $OPPh_3$ with parallel quantitative formation of complex **1a**. Oxygen transfer activity was also observed upon reaction with CO. When **2** was treated with 4 equivalents of CO gas, it was quantitatively transformed into the cationic carbonyl complex **1b** with concomitant formation of CO_2 (83% yield) as determined by gas chromatography. Complex **2** also reacts with hydrogen. Stirring **2** under 5 atm of H_2 led to deoxygenation, forming complex **1a** in 52% yield, with complex **3** (see later) being a competitive product. Mechanistic studies of H_2 oxidation by MnO_4^- and RuO_4 have been reported[24].

Complex **2** can also be attacked by nucleophiles. Addition of KH to a THF solution of **2** resulted in formation of the reported[20] Pt(II) hydroxo complex **1c**, probably by hydride attack at the metal centre, followed by its migration to the oxo ligand (Fig. 3). Complex **1c** constitutes 78% of the organometallic products (see Supplementary Information).

Complex **2** is only moderately thermally stable. After 7–10 h at room temperature, in the absence of an external oxygen acceptor, it undergoes intramolecular oxygen transfer, resulting in insertion of the oxo ligand into the Pt–P bond to give the new complex **3** (Fig. 3). Complex **3** was fully characterized by multinuclear NMR spectroscopy. The $^{31}P\{^1H\}$ NMR spectrum of **3** exhibits a singlet at 76.57 p.p.m. with a very small Pt–P coupling constant (40 Hz) due to oxygen incorporation. The ^{195}Pt NMR spectrum exhibits a singlet at −2,842.87 p.p.m. Colourless needles of **3** suitable for a single-crystal X-ray diffraction study were obtained from an acetone/pyridine solution by slow vapour diffusion of ether at room temperature (Fig. 4a). Complex **3** (solv = pyridine) exhibits a slightly distorted square planar structure. The oxygen atom is bound to the Pt and P atoms, and the Pt–O length (2.031 Å) indicates a single-bond character, while the P–O bond length of 1.529 Å is short enough to be considered a double bond (based on the Cambridge Structural Database). Results of DFT calculations on the structure of complex **3** are in good agreement with the X-ray data. The geometries of

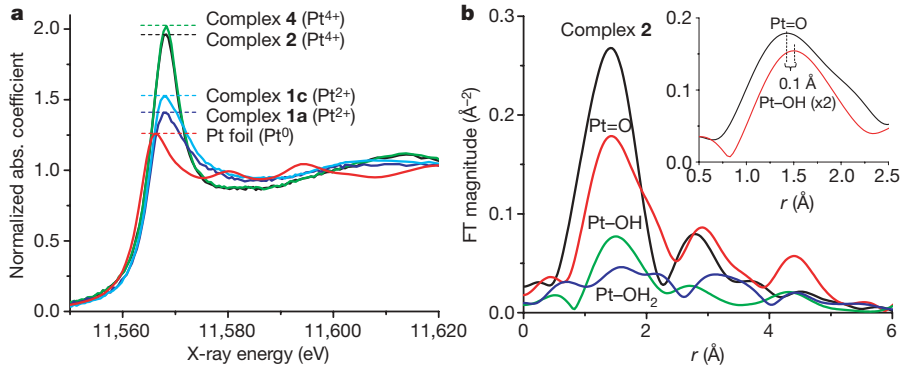

Figure 2 | XANES spectra of complexes and Fourier transform magnitudes of EXAFS data. a, XANES spectra for complex **2** and reference complexes **1a** (solv = H_2O), **1c**, **2** and **4**. **b**, Fourier transform (FT) magnitudes, uncorrected for photoelectron phase shifts, of k-weighted EXAFS data for complex **2** and individual contributions Pt=O, Pt–OH and Pt–OH_2. Inset, the ~0.1 Å shift to lower distances of the Pt=O peak relative to Pt–OH (the latter peak is scaled up by a factor of 2 for clarity).

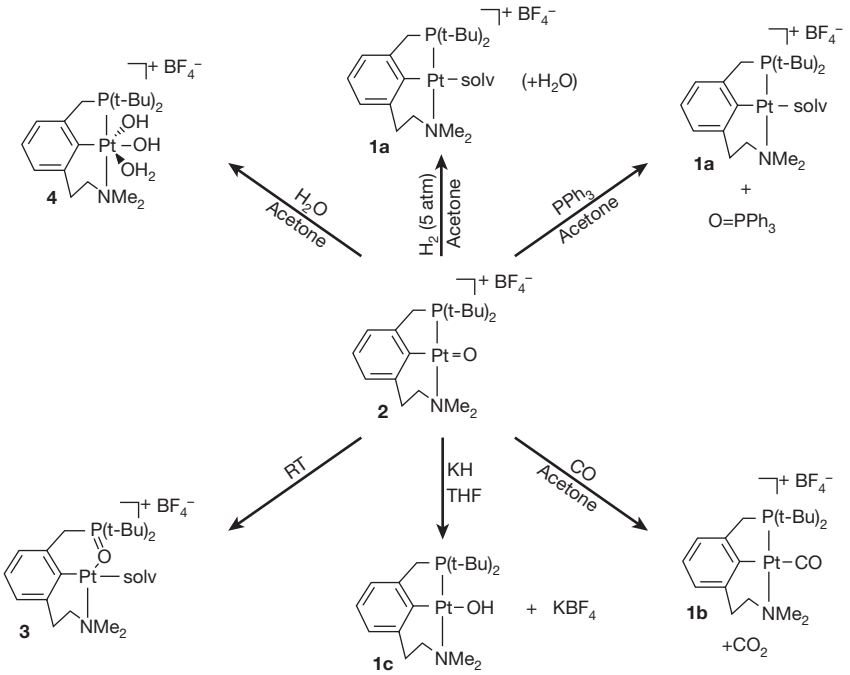

Figure 3 | Reactivity of complex 2. Oxygen transfer to H_2 and to PPh_3 with reduction to the Pt(II) complex **1a**; oxygen transfer to CO forming complex **1b** and CO_2; intramolecular oxo transfer to form complex **3**; nucleophilic attack by a hydride, generating the Pt(II) hydroxo complex **1c**; and water activation to form the dihydroxo Pt(IV) complex **4**.

complexes **2**, **3** and **4** were optimized at the same level of theory. The observed good correlation between theoretical and X-ray single-crystal data for **3** and **4** (Supplementary Tables 2 and 3) lends credence to the calculated geometry of complex **2**.

Terminal oxo intermediates are implicated as key intermediates in the artificial catalytic water oxidation to O_2, the mechanism of which is a subject of numerous theoretical and experimental studies[25–28], although the nature of the step leading to the generation of dioxygen is not clear[9–13]. In this context, it is desirable to know how a late transition metal terminal oxo complex reacts with water. Interestingly, when excess water was added to **2**, the new dihydroxo Pt(IV) complex **4** was immediately formed (Fig. 3). Complex **4** was fully characterized by multinuclear NMR and mass spectroscopy (see Supplementary Information). Colourless crystals of **4** suitable for X-ray diffraction analysis were obtained from a CH_2Cl_2 solution at −30 °C (Fig. 4b). Complex **4** has a classical octahedral structure, the Pt atom being coordinated to the PCN ligand and to three oxygen atoms. The Pt–O bond lengths are 1.997(5), 2.017(5) and 2.171(5) Å for atoms O1, O2 and O3, respectively. Lacking the Pt=O functionality, and being significantly more stable than **2**, complex **4** does not exhibit oxygen transfer reactivity and remains unchanged for weeks upon addition of PPh_3.

We are unaware of prior direct observations of water activation by a terminal oxo complex, and trapping of the product of such activation. It is noteworthy that oxidation of Pt(II) to Pt(IV) by O_2 in water to generate a Pt(IV) dihydroxo complex is proposed as a key step in a hypothetical catalytic cycle for alkane oxidation by O_2 to give alcohols[29,30]. Our results suggest that such a process might involve O–H activation of water by a Pt(IV) oxo intermediate. DFT calculations show that in our system such activation is very favourable. Upon addition of two water molecules to the apical positions of the oxo complex **2**, geometry optimization gave the dihydroxo structure **4**. The calculated free energy change of this reaction is $\Delta G^{\circ}_{298} = -19.8$ (-20.6) kcal mol^{-1} in acetone (water) solution.

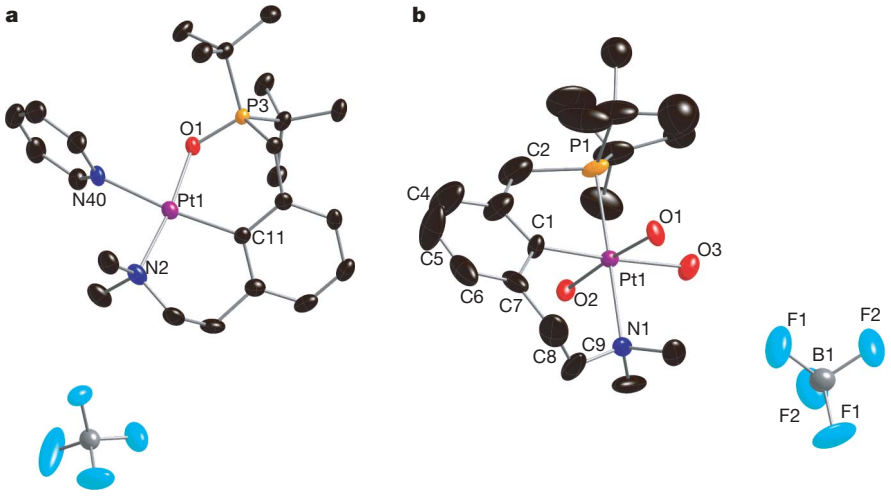

Figure 4 | ORTEP views of molecules of 3 and 4 with the thermal ellipsoids at 50% probability. a, **3**; **b**, **4**. Hydrogen atoms were omitted for clarity (OH hydrogen atoms of complex **4** were not located).

Received 14 March; accepted 20 August 2008.

1. Nugent, W. A. & Mayer, J. M. *Metal-Ligand Multiple Bonds* (Wiley, 1988).
2. Holm, R. H. Metal-centered oxygen atom transfer reactions. *Chem. Rev.* **87,** 1401–1449 (1987).
3. Sheldon, R. A. & Kochi, J. K. *Metal-Catalyzed Oxidations of Organic Compounds* (Academic, 1981).
4. Meunier, B. (ed.) *Biomimetic Oxidations Catalyzed by Transition Metal Complexes* (Imperial College Press, 2000).
5. Yoshizawa, K. Nonradical mechanism for methane hydroxylation by iron-oxo complexes. *Acc. Chem. Res.* **39,** 375–382 (2006).
6. Rohde, J.-U. *et al.* Crystallographic and spectroscopic characterization of a nonheme Fe(IV)-O complex. *Science* **299,** 1037–1039 (2003).
7. Green, M. T., Dawson, J. H. & Gray, H. B. Oxoiron(IV) in chloroperoxidase compound II is basic: Implications for P450 chemistry. *Science* **304,** 1653–1656 (2004).
8. Somorjai, G. A. *Introduction to Surface Chemistry and Catalysis* (Wiley, 1994).
9. Ruettinger, W. & Dismukes, G. C. Synthetic water-oxidation catalysts for artificial photosynthetic water oxidation. *Chem. Rev.* **97,** 1–24 (1997).
10. Yagi, M. & Kaneko, M. Molecular catalysts for water oxidation. *Chem. Rev.* **101,** 21–35 (2001).
11. Alstrum-Acevedo, J. H., Brennaman, M. K. & Meyer, T. J. Chemical approaches to artificial photosynthesis. 2. *Inorg. Chem.* **44,** 6802–6827 (2005).
12. Dempsey, J. L. *et al.* Molecular chemistry of consequence to renewable energy. *Inorg. Chem.* **44,** 6879–6892 (2005).
13. Lewis, N. S. & Nocera, D. G. Powering the planet: Chemical challenges in solar energy utilization. *Proc. Natl Acad. Sci. USA* **103,** 15729–15735 (2006).
14. Spaltenstein, E., Conry, R. R., Critchlow, S. C. & Mayer, J. M. Low-valent rhenium-oxo complexes. 9. Synthesis, characterization, and reactivity of a formally rhenium(I) terminal oxo complex, $NaRe(O)(RC{\equiv}CR)_2$. *J. Am. Chem. Soc.* **111,** 8741–8742 (1989).
15. Anderson, T. M. *et al.* Late-transition metal oxo complex: $K_7Na_9[O:Pt^{IV}(H_2O)L_2]$, $L = [PW_9O_{34}]^{9-}$. *Science* **306,** 2074–2077 (2004).
16. Anderson, T. M. *et al.* Palladium-oxo complex. Stabilization of this proposed catalytic intermediate by an encapsulating polytungstate ligand. *J. Am. Chem. Soc.* **127,** 11948–11949 (2005).
17. Cao, R., Musaev, D. J., Morokuma, K., Takahashi, M. & Hill, C. L. Terminal gold-oxo complexes. *J. Am. Chem. Soc.* **129,** 11118–11133 (2007).
18. MacBeth, C. E. *et al.* O_2 activation by nonheme iron complexes: A monomeric Fe(III)-oxo complex derived from O_2. *Science* **289,** 938–941 (2000).
19. Van der Boom, M. E. & Milstein, D. Cyclometalated phosphine-based pincer complexes: Mechanistic insight in catalysis, coordination, and bond activation. *Chem. Rev.* **103,** 1759–1792 (2003).
20. Poverenov, E. *et al.* Pincer ''hemilabile'' effect. PCN platinum(II) complexes with different amine ''arm length''. *Organometallics* **24,** 1082–1090 (2005).
21. Murray, R. W. & Singh, M. Chemistry of dioxiranes. Reaction of dimethyldioxirane with alkynes. *J. Org. Chem.* **58,** 5076–5080 (1993).
22. Sassenberg, U. & Scullman, R. The emission spectrum of PtO between 3800 A and 8900 A. *Phys. Scripta* **28,** 139–159 (1983).
23. Schott, D., Pregosin, P. S., Albinati, A. & Rizatto, S. PGSE diffusion NMR studies on mononuclear and dinuclear cationic salts of (*S*)-MeO-Biphep and (*R*)-*p*-tolyl-BINAP. *Inorg. Chim. Acta* **360,** 3203–3212 (2007).
24. Collman, J. P., Slaughter, L. M., Eberspacher, T. A., Strassner, T. & Brauman, J. I. Mechanism of dihydrogen cleavage by high-valent metal oxo compounds: Experimental and computational studies. *Inorg. Chem.* **40,** 6272–6280 (2001).
25. Yang, X. & Baik, M.-H. *cis,cis*-$[(bpy)_2Ru^{V}O]_2O^{4+}$ catalyzes water oxidation formally via in situ generation of radicaloid Ru^{IV}-O*. *J. Am. Chem. Soc.* **128,** 7476–7485 (2006).
26. Hurst, J. K. Water oxidation catalyzed by dimeric μ-oxo bridged ruthenium diimine complexes. *Coord. Chem. Rev.* **249,** 313–328 (2005).
27. Elizarova, G. L., Zhidomirov, G. M. & Parmon, V. N. Hydroxides of transition metals as artificial catalysts for oxidation of water to dioxygen. *Catal. Today* **58,** 71–88 (2000).
28. Binstead, R. A., Chronister, C. W., Ni, J., Hartshorn, C. M. & Meyer, T. J. Mechanism of water oxidation by the μ-oxo dimer $[(bpy)_2(H_2O)Ru^{III}ORu^{III}(OH_2)(bpy)_2]^{4+}$. *J. Am. Chem. Soc.* **122,** 8464–8473 (2000).
29. Labinger, J. A. & Bercaw, J. E. Understanding and exploiting C–H bond activation. *Nature* **417,** 507–513 (2002).
30. Rostovtsev, V. V., Labinger, J. A., Bercaw, J. E., Lasseter, T. L. & Goldberg, K. I. Oxidation of dimethylplatinum(II) complexes with dioxygen. *Organometallics* **17,** 4530–4531 (1998).

Supplementary Information is linked to the online version of the paper at www.nature.com/nature.

Acknowledgements This research was supported in part by the Israeli Science Foundation, by the German Federal Ministry of Education and Research (BMBF) under the framework of the German-Israeli Cooperation, by the Minerva Foundation, Munich, Germany, and by the Helen and Martin Kimmel Center for Molecular Design. A.I.F. acknowledges support from the US Department of Energy (DE-FG02-03ER15476). Beamline X18B is supported by the NSLS through the Divisions of Materials and Chemical Sciences of the US DOE, and the Synchrotron Catalysis Consortium through the US DOE (DE-FG02-05ER15688). We thank Q. Wang for help with the synchrotron measurements. D.M. holds the Israel Matz Professorial Chair.

Author Contributions E.P.: synthesis, characterization, reactivity studies of complexes and manuscript writing. I.E. and J.M.L.M.: DFT calculations and manuscript writing. A.I.F.: X-ray absorption spectroscopy studies. Y.B.-D.: synthesis of the PCN ligand and dioxirane. L.J.W.S. and G.L.: single-crystal X-ray diffraction analysis. L.K.: NMR studies. D.M.: design and direction of the project and manuscript writing.

Author Information Crystallographic data for complexes **3** and **4** have been deposited in the Cambridge Crystallographic Data Centre, under accession numbers 695884 and 695883, respectively. Reprints and permissions information is available at www.nature.com/reprints. Correspondence and requests for materials should be addressed to D.M. (david.milstein@weizmann.ac.il).